Journal of Materials Chemistry A

Accepted Manuscript

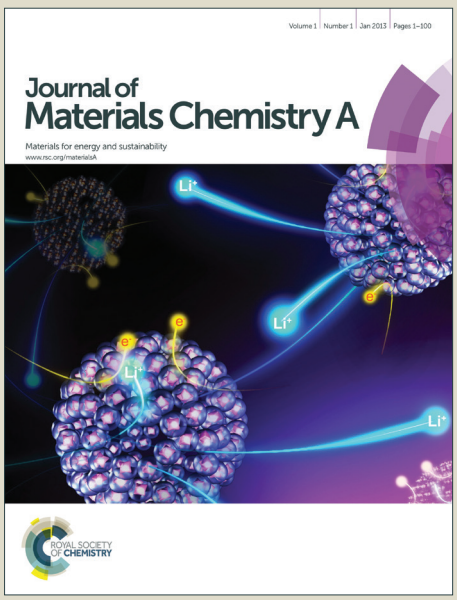

ROYAL SOCIETY OF CHEMISTRY

www.rsc.org/materialsA

Cite this: DOI: 10.1039/c0xx00000x

www.rsc.org/xxxxxx

ARTICLE TYPE

A distinctive red Ag/AgCl photocatalyst with efficient photocatalytic oxidative and reductive activity

Bin Cai,[a,c] Jing Wang,[b,c] Shiyu Gan,[a,c] Dongxue Han,[a] Zhijian Wu,[b] and Li Niu*[a]

Received (in XXX, XXX) Xth XXXXXXXXX 20XX, Accepted Xth XXXXXXXXX 20XX

DOI: 10.1039/b000000x

Optical absorption, as the fundamental requirement of photocatalysts, still has an immense space for development. Herein, we design a novel kind of red Ag/AgCl photocatalyst, upon which a large improvement of visible-light harvesting was obtained. This strongly coloured semiconductor materials can be facilely prepared using a versatile glycerol-mediated method and exhibit a uniform coaxial tri-cubic morphology. The enhancement of optical absorption is not only ascribed to the synergy of Ag and AgCl but also attributed to the Mie scattering effect due to the distinct morphology. As expected, the as-prepared red Ag/AgCl photocatalysts exhibit highly enhanced photocatalytic activities in the degradation of organic dye, reduction of hexavalent chromium and conversion of CO_2 into liquid hydrocarbon fuels. By means of theoretical calculations, furthermore, this work provides an in-depth perspective for understanding the physical photocatalytic mechanism of the red Ag/AgCl system and should stimulate the development of silver halide-based photocatalysts for the exploitation and utilization of solar energy.

Introduction

Plasmonic photocatalysis has recently come into focus as a very promising technology for high-performance photocatalysis.[1-4] Although it could be traced back to the works of Kamat's group[5, 6] and others[7], the term 'plasmonic' was coined by Awazu and co-workers[8] until 2008. The two main characteristics of plasmonic photocatalysis due to the incorporation of noble metal (Ag, Au, Pt, *et al*.) nanoparticles (NPs) are the Schottky junction and the localized surface plasmon resonance (LSPR).[1, 9-12] The separation of photo-induced charge carries, one of the most crucial factors for an ideal photocatalyst, can be promoted by the intensive electric field inside the space charge region due to the Schottky junction.[10, 13] The LSPR effect can not only drastically arouse and enhance the visible-light harvesting of both large-[12] and low-[14] bandgap photocatalysts, but also create an intensive local electric field which facilitates the photocatalytic reactions significantly.[15] To date, assembled hybrid nano-structures of plasmonic Ag,[8, 16, 17] Au,[12, 18, 19] and Pt[20-22] NPs on various semiconductors have been extensively studied and they exhibit strong plasmon-excitation coupling interactions under light irradiation, giving rise to many encouraging effects.[1, 23]

Unlike the traditional noble metal/semiconductor plasmonic systems, silver halide materials (AgX, X=Cl, Br and I), as photosensitive semiconductors which remain stable after the preliminary decomposition into Ag^0 species under irradiation,[24] are found to be one of the most promising plasmonic photocatalysts.[11, 25-28] As reported, AgX-based nanomaterials with various morphologies, including nano-cubes,[27] spheres,[29] wires,[30] cages,[31] octahedras,[32] films,[33] and other shapes,[26, 28, 34] have been widely studied in terms of the specific properties and corresponding potential applications. Moreover, many attempts have also been made to organize AgX/semiconductor hierarchical composites, such as AgX/Ag_3PO_4,[35] $AgBr/TiO_2$,[36] $AgBr/WO_3$,[37] AgI/Al_2O_3,[16] *etc*.[1, 2, 4] However, most methods reported to date are of limited use in practice due to the higher engineering requirements. Recently, to further improve the AgX-based photocatalysis, our group has also introduced sulfonated graphene (SGE) into the Ag/AgBr system, and in this work, SGE enhances the transfer and separation of photoinduced charge carriers significantly due to its unique energy band dispersion and low Fermi level.[10] Inspired by the theoretical prediction of the bandgap engineering of AgX-based alloys,[38] we have also successfully realized the manipulation of electronic structure of AgX nanocrystals and the energy band dependent photocatalytic activities have further been investigated and demonstrated based on the experimental results and theoretical calculations.[39] During this series study, we were surprised to find a novel kind of red Ag/AgCl photocatalysts by accident. The deep colour indicates a strong visible-light harvesting ability and should have promising potential for improving the AgX photocatalysis.

In this work, we describe the synthesis and characterizations of this novel kind of red Ag/AgCl photocatalysts which can be prepared through a facile and versatile approach and possesses uniform coaxial tri-cubic morphology. The as-prepared red photocatalysts exhibit intrinsic high absorption in the visible and even infrared region, which is crucial for improved photocatalysis. The optical absorption of the as-prepared Ag/AgCl photocatalysts is greatly enhanced not only by the LSPR effect but also by Mie scattering effect of the Ag/AgCl NPs. Their photocatalytic oxidative and reductive abilities are evaluated in terms of the degradation of methyl orange (MO),

reduction of hexavalent chromium and conversion of CO_2 into methanol and ethanol, respectively. Results show that the as-prepared red Ag/AgCl photocatalysts exhibit higher photocatalytic oxidative and reductive activity than both normal Ag/AgCl and TiO_2 materials. With the aid of density functional theory (DFT), physical photocatalytic mechanism of the red Ag/AgCl system is further demonstrated.

Experimental

Synthesis of coaxial tri-cubic Ag/AgCl red NPs

The red Ag/AgCl NPs were synthesized by a glycerol-mediated method according to previous reports with some modifications.[28, 40] In a typical procedure, PVP (108 mg), NaCl (22 mg) were dissolved in glycerol (15 mL) in a 50 mL round-bottom flask at 40 ^oC under stirring for 15 min (the solution transformed to pellucid). Then the mixture was heated to 60 ^oC and 2 mL of glycerol solution (containing 52 mg $AgNO_3$, dissolved at room temperature under stirring) was injected slowly into the reaction solution. The reaction was then maintained at 60 ^oC for 1 h, and finally a milky dispersion was obtained. Afterwards, the reaction system was warmed up to 140 ^oC at a heating rate of 2 ^oC min^{-1} (within 40 min) and maintained at this temperature for another 20 min before it was cooled down to room temperature naturally. Finally, the reddish-brown suspension was treated by centrifugation (10000 rpm, 5 min) to collect the resulted red NPs and rinsed thoroughly first with acetone and then with water several times (at least 3 times). For comparison, normal Ag/AgCl materials are prepared by mixing aqueous $AgNO_3$ (0.01 mol L^{-1}) and NaCl (0.01 mol L^{-1}) solution directly under stirring.

Evaluation of photocatalytic activities

For the photodegradation experiments, the photocatalysts (50 mg) were suspended in 50 mL of MO solution (10 mg L^{-1}) by sonication. Before the degradation reaction was carried out, the dispersion was kept stirring in the dark for preliminary adsorption (30 min). The light source was a 500 W xenon arc lamp (CHF-XM35-500w, Beijing Trusttech Co. Ltd, China) equipped with a UV cut filter ($\lambda > 420$ nm). Specified dispersions (600 μL) were pipetted from the reaction system for real-time investigations at certain time intervals. The concentration of MO was monitored by the UV-Vis spectroscopy *via* recording the absorbance of the characteristic peak of MO at 463 nm where C and C_0 refer to the concentrations of MO at real time *t* and at 10 mg L^{-1}, respectively.

The photoreduction of the Cr^{VI} was performed with Ag/AgCl photocatalysts (20 mg) suspended in 19 mL of K_2CrO_4 solution (15 mg L^{-1}). The light source was the same as the degradation reaction. The concentration of dissolved Cr^{VI} was determined colorimetrically based on the diphenylcarbazide (DCP) method. In a typical procedure, 0.5 mL of ethylene diamine tetraacetic acid solution (EDTA, 4 mg mL^{-1}) was added as the sacrificial reagent, and the pH of the reaction suspension was adjusted to 2 with dilute $HClO_4$ (20-fold dilution). Then DCP solution (0.5 mL, 5 mg mL^{-1} in acetone) was added to develop a red-violet colour. The Cr^{VI} concentration was measured by recording the absorbance of the characteristic peak at 540 nm by the UV-Vis spectroscopy. C and C_0 refer to the concentrations of Cr^{VI} at real time t and at 15 mg L^{-1}, respectively.

The photoreduction of CO_2 into liquid fuels was carried out on a home-made reactor (see ESI, Fig. S1†). In a typical process, the photocatalysts (15 mg) were dispersed in $NaHCO_3$ solution (15 mL, 0.1 mol L^{-1}) *via* 10 min of sonication. Prior to the irradiation (light source was the same as the degradation reaction), ultrahigh purity CO_2 was bubbled through the suspended solution at a rate of 0.7 L min^{-1} for 10 min to remove the air and saturate the solution with CO_2. After reacting for 5 h, the suspension was centrifuged to collect the catalyst, and the product was analyzed using a gas chromatograph (Agilent GC 6890N, FID detector). The apparent quantum efficiency (AQE) is evaluated in terms of the ferrioxalate actinometer method,[28, 41, 42] and the details was described in the ESI†.

Theoretical calculations

The electronic structure of the AgCl material was calculated by the WIEN2K program,[43, 44] based on the full-potential linearized augmented plane wave (FP-LAPW) method. The exchange-correlation (xc) energy was treated by the generalized gradient approximation of Perdew-Burke-Ernzenhof (GGA-PBE).[45] The plane wave expansion cutoffs were 7.0 for the expanding wave function (RKMAX). 1000 k-points were used in the complete Brillouin zone. The self-consistent calculations were considered to be converged when the energy difference is less than 10^{-5} Ry. Since GGA often underestimates the band-gap values, onsite Coulomb interaction or electron correlation (U) for Ag 4d was considered in the rotationally invariant way.[46] A series of U values (8.00-13.92 eV) had been tested. We employed the results from U=13.92eV for discussion which was also adopted for Ag_3PO_4 in previous calculation.[47]

Results and discussion

Synthesis, characterization and photophysical properties

Glycerol has been found to be a favourable reaction medium to design uniformly shaped nanomaterials due to its high viscosity at low temperature, which herein may significantly reduce the diffusion coefficients of both Ag^+ and Cl^- ions to slow down the precipitation reaction.[28] Under this principle, strongly colored Ag/AgCl NPs with uniform coaxial tri-cubic morphology can be facilely prepared by controlling the reaction temperature and time (Fig. 1A). PVP herein serves as a capping agent to stabilize the resulting AgCl NPs and prevent the agglomeration. Further, the polymeric chains of PVP also enhance the overall viscosity of the reaction solution and facilitate the morphology control of Ag/AgCl NPs. The strong reducibility of glycerol at high temperature promotes the generation of Ag^0 species on the surface of AgCl NPs. Typical SEM images of the as-prepared Ag/AgCl NPs before and after the photocatalysis reaction are presented in Fig. 1 and Fig. S2-S3 (see ESI†). As shown in the SEM images, the as-prepared Ag/AgCl NPs display similar diameters of 500-600 nm and uniform coaxial tri-cubic morphology with smooth surfaces (Fig. 1F-G). The digital image (Fig. 1E) of the dispersion of the red Ag/AgCl sample (1 mg mL^{-1}) reveals the megascopic red colour of the red AgCl sample, which is remarkably different from the commonly observed milky white AgCl NPs (see ESI, Fig. S5†).

The crystal structure of the red Ag/AgCl sample is examined by means of XRD (Fig. 2A). The XRD pattern of the Ag/AgCl

sample displays distinct diffraction peaks (2θ) at 27.8° (111),

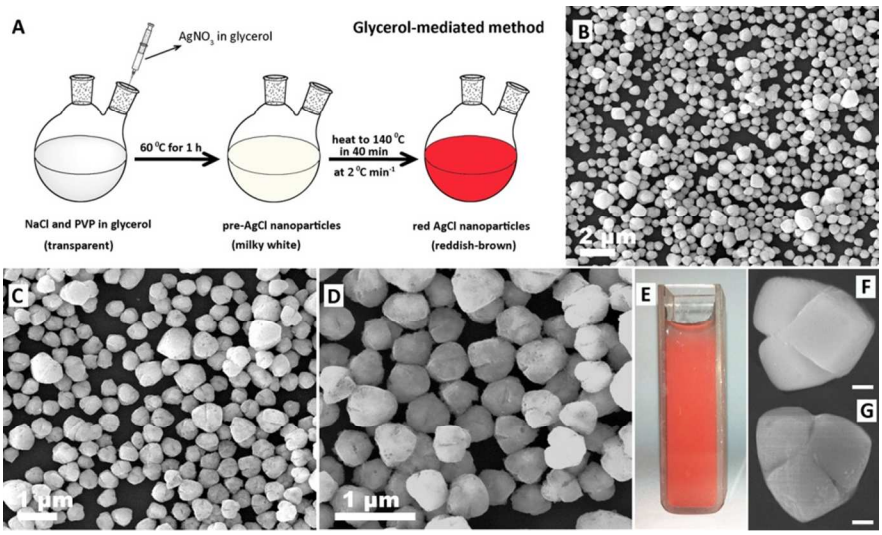

Fig. 1 Synthesis procedure, photographs and SEM images of the red Ag/AgCl NPs. A) Schematic illustration of the synthesis of the red Ag/AgCl NPs, B-D) SEM images of the as-prepared Ag/AgCl NPs with different resolutions, E) digital image of the red AgCl dispersion, and F-G) a magnified image for a clearer view of the coaxial tri-cubic morphology. The scale bar is 100 nm.

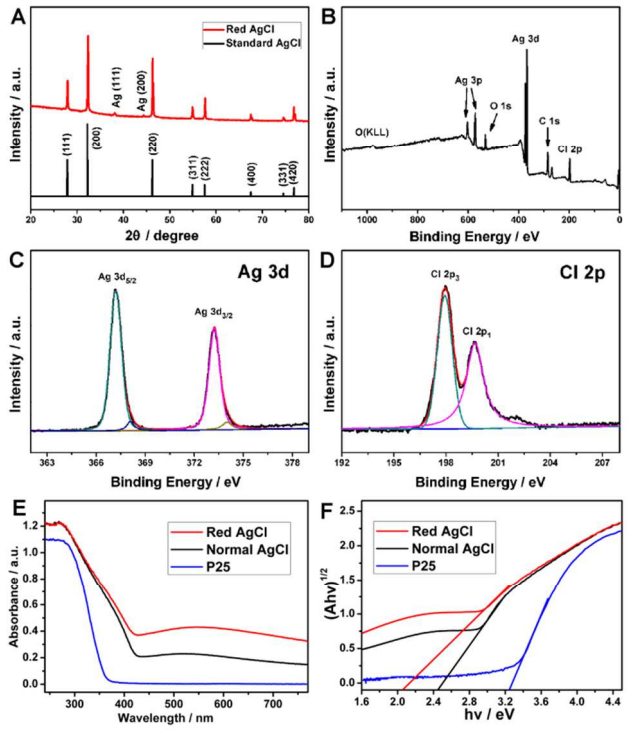

Fig. 2 XRD and XPS characterizations and photophysical properties of the red Ag/AgCl photocatalysts. A) XRD patterns of red Ag/AgCl sample in comparison with AgCl (JCPDS file: 31-1238), the survey XPS spectrum B), Ag3d C) and Cl 2p D) of the red Ag/AgCl sample, E) UV-Visible diffuse reflectance spectra of the red Ag/AgCl NPs, normal AgCl and commercial TiO_2 (P25), and F) the corresponding bandgap estimation based on the Kubelka-Munk Theory.

32.2° (200), 46.2° (220), 54.8° (311), 57.5° (222), 67.5° (400), 74.5° (331), and 76.8° (420), which correspond well to the diffractions of crystalline AgCl (JCPDS file: 31-1238). Additionally, we note that the diffraction peaks (2θ) at 38.1° (111), 44.3° (200) are indexed to the metallic Ag (JCPDS file: 65-2871), indicating that Ag^0 nanospecies are produced on the surface of AgCl. This can be partially ascribed to the strong reducibility of glycerol at high temperature, which facilitates the generation of Ag^0 nanospecies during the synthesis procedure. The lattice parameter of the red Ag/AgCl NPs is calculated to be 5.55 Å, which is also equal to the theoretical values (5.549 Å).[48] Further, no characteristic peaks belonging to impurities or other phases are detected, indicating that the as-obtained product is solely composed of metallic Ag and AgCl.

The surface chemical composition and chemical states of the as-prepared samples are confirmed by XPS spectroscopy (Fig. 2B-D). As shown in the survey XPS spectrum (Fig. 2B), the peaks of Ag, Cl, C, and O can be obviously detected. The carbon and oxygen peaks are largely attributed to the adventitious impurities from the XPS instrument itself. Fig. 2C presents the characteristic Ag 3d bands. The two bands at *ca.* 367.2 and 373.2 eV can be attributed to the Ag $3d_{5/2}$ and $3d_{3/2}$ binding energies respectively. Furthermore, the peaks of Ag $3d_{5/2}$ and $3d_{3/2}$ could be deconvoluted into peaks at 367.2, 368.2 eV and 373.2, 374.2 eV, respectively. The peaks at 368.2 and 374.2 eV are attributed to metallic Ag^0, whereas the peaks at 367.2 and 373.2eV are for Ag^+ inside AgCl. The XPS spectra of Cl 2p (Fig. 2D) display two bands at *ca.* 197.9 and 199.6 eV, which are fitted with Cl $2p_1$ and $2p_3$ binding energies respectively.

Generally, materials can only be strongly coloured if they strongly absorb light.[49] The optical absorption of the as-prepared Ag/AgCl photocatalysts is herein demonstrated by the UV-Vis diffuse reflectance spectra (Fig. 2E). Commonly, due to the large bandgap (about 3.2 eV), bare AgCl materials show negligible absorption in the visible region.[11, 27] Compared with TiO_2 (P25), however, both the two types of AgCl materials show distinct absorptions in the visible region. The enhancement could be assertively attributed to the collective electronic oscillation by LSPR of the Ag^0 species. More importantly, the as-prepared red Ag/AgCl samples absorb more energy in the visible region than

normal Ag/AgCl materials. The main reason could be attributed to the increased quantity of Ag^0 species on the surface of red AgCl NPs than common AgCl materials (see ESI, Fig. S6†). In addition, the Mie scattering effect cannot be ignored. Owing to the unique coaxial tri-cubic morphology of the red Ag/AgCl NPs, the photon path length in the surface of the semiconductor is significantly increased, which also enhances the optical adsorption. And the Mie scattering could also facilitate the generation of metallic Ag, which supports the LSPR effect in turn. Fig. 2F reveals the corresponding bandgap estimation based on the Kubelka-Munk Theory. The as-prepared Ag/AgCl sample show smaller apparent bandgap value than normal Ag/AgCl and TiO_2 materials, which further demonstrates the enhanced optical absorption capacity.

Evaluation of photocatalytic activity

The photocatalytic oxidative and reductive performances of the as-obtained Ag/AgCl photocatalysts are evaluated quantitatively by degradation of methyl orange (MO) dye, reduction of Cr^{VI} and conversion of CO_2 into liquid hydrocarbon fuels under visible light irradiation (Fig. 3). The degradation dynamic curves of MO over different photocatalysts are shown in Fig. 3A. The real-time concentration variation of MO (C/C_0, C_0 = 10 mg L^{-1}) is measured by means of the normalized absorption value (A/A^0, λ = 463 nm) at the given time intervals (see ESI, Fig. S7†).[10] Prior to irradiation, the reaction system was kept in the dark for 30 min to reach an adsorption equilibrium state. As the degradation process follows a pseudo-first-order reaction, we calculated the corresponding degradation rate constant (k_{MO}) in terms of the sudden drops of the MO concentration occurring over the first 2 min irradiation. The red Ag/AgCl photocatalysts exhibit efficient activity (k^R_{MO} = 0.39 min^{-1}), twice higher than normal Ag/AgCl materials (k^N_{MO} = 0.16 min^{-1}). As shown in Fig. 3A, the MO solution can be decolorized completely with the red Ag/AgCl NPs as catalyst after exposure to visible-light irradiation for 8 min. The HPLC analysis further confirmed the photodegradation of MO (see ESI, Fig. S11†).

Carcinogenic hexavalent chromium is the primary pollutant in chromium–containing waste water. As the toxicity of chromium is related to its oxidation states, transforming it to a more benign form represents an effective approach to handle the pollution. As reported, reduction of Cr^{VI} into Cr^{III} has been accomplished many times *via* photocatalysis.[25, 50] As shown in Fig. 3B, the Cr^{VI} concentration decreased gradually with increasing irradiation time and the as-obtained red Ag/AgCl photocatalysts exhibit higher activities for Cr^{VI} reduction than both normal Ag/AgCl and TiO_2 under visible irradiation. The real-time concentration variation of the dissolved Cr^{VI} is determined colorimetrically by the normalized absorption value (A/A^0, λ = 540 nm, see ESI, Fig. S8†) by means of the reaction with diphenylcarbazide (DCP) in acid solution. The results indicate that almost all of the Cr^{VI} was reduced after irradiation for 12 min upon the red Ag/AgCl photocatalysts, while only 78% and 15% of Cr^{VI} was detoxified upon normal AgCl and TiO_2 materials. Blank experiments without irradiation and experiments in the absence of photocatalyst demonstrate that the concentration of hexavalent chromium remained unchanged. The reduction of Cr^{VI} manifests the efficient photocatalytic reductive activity of the as-obtained red Ag/AgCl NPs.

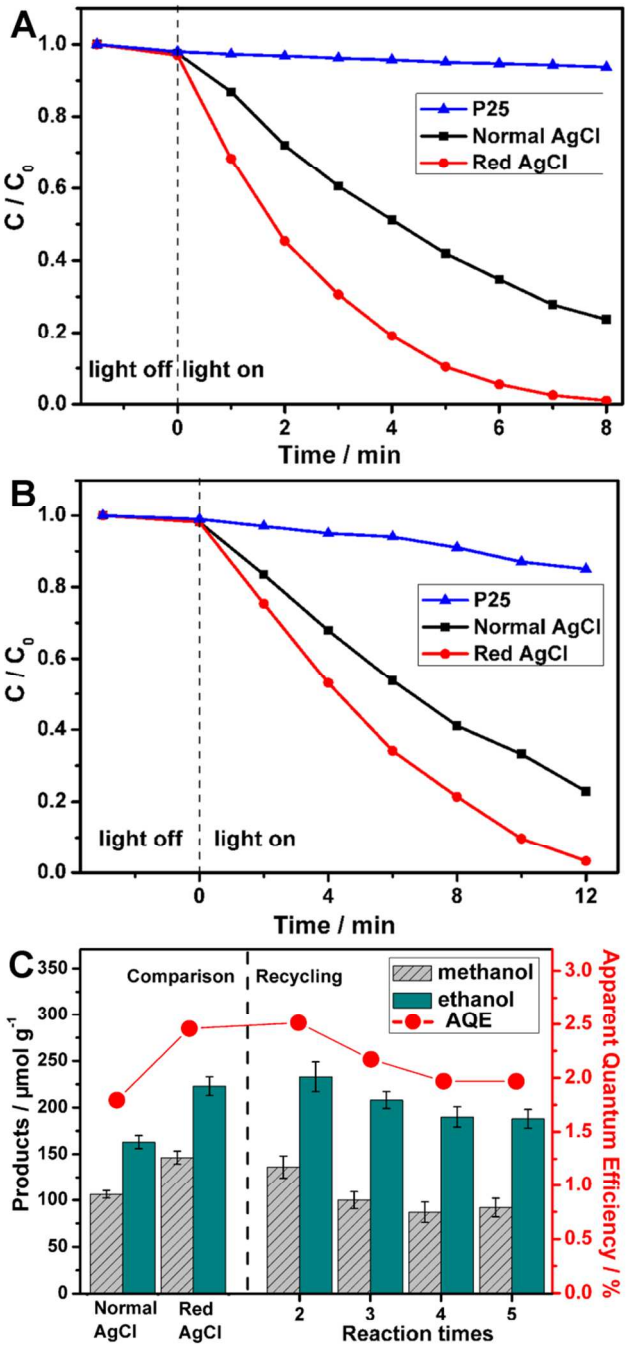

Fig. 3 Evaluation of the photocatalytic performances. Reaction dynamic curves of MO A) and Cr^{VI} B) over the red Ag/AgCl photocatalysts, normal Ag/AgCl material and TiO_2, C) comparison and recycling experiments of the product yields and the corresponding AQE upon the red Ag/AgCl photocatalysts.

Among the numerous methods developed so far, photocatalytic reduction of CO_2 into liquid hydrocarbon fuels represents a promising strategy to deal with the greenhouse effect and energy crisis. However, the pioneering of highly efficient CO_2 photoreduction still remains a challenging task. Silver halides have been proven to be promising materials to reduce CO_2 under visible light irradiation due to the more negative conduction band (CB) edges than $\varphi^{\ominus}(CO_2/CH_3OH)$ and $\varphi^{\ominus}(CO_2/C_2H_5OH)$ (-0.38 and -0.085 eV *vs.* NHE).[28, 51] Herein, the photo-reductive ability

of the as-prepared red Ag/AgCl NPs has also been evaluated in terms of CO_2 reduction. Comparison of the photocatalytic product yields of the as-prepared red Ag/AgCl NPs and normal AgCl materials is shown in Fig. 3C. The methanol and ethanol yields upon the red Ag/AgCl samples are 146 and 223 μmol g^{-1}, both of which are higher than those of normal AgCl materials (106 and 163 μmol g^{-1} for methanol and ethanol, respectively). Furthermore, we measured the apparent quantum efficiency (AQE) of the CO_2 reduction reaction in terms of the ferrioxalate actinometer method (Fig. 3C).[41] The results show that the AQE of the red Ag/AgCl samples reaches 2.46%, higher than the normal AgCl materials (1.79%). For comparison, experiments without catalyst and without light irradiation were also carried out, and no organic matter could be detected.

For the purpose of practical application, the stability of the as-prepared red Ag/AgCl photocatalysts was also evaluated in terms of recycling the photocatalysts several times for the three types of photocatalytic reactions (see ESI, Figs. S9-10† and Fig. 3C). The slight shrinkage of catalytic activity can be attributed to a small loss of the catalyst during the cycling reaction. These results manifest the chemical stability of the red Ag/AgCl photocatalysts.

Physical photocatalytic mechanism

To provide in-depth physical perspective into the activity of the red Ag/AgCl photocatalysts, the band structure and densities of states (DOS) of AgCl were calculated using DFT (Fig. 4 and Fig. S12-13†). According to the calculated DOS (see ESI, Figs. S12-13†), both the conduction and valence band (CB and VB) of the AgCl material are composed of Cl 3p and Ag 4d states, whereas Ag 4d states contribute little to the composition of CB. And because of the participation of Ag 4d states in the construction of valence band maximum (VBM) which could induce relatively localized photoholes, AgCl material can be referred to as typical electron-conductive semiconductor. As shown in the energy-band diagram (Fig. 4), AgCl material is found to be an indirect bandgap semiconductor, and the indirect electronic transition can be seen from L to Γ point with a bandgap value of 2.8 eV. Due to the favourable CB level, there occurs a strong electronic coupling between the CB of Ag^0 species and AgCl semiconductor, thus greatly promotes the photoinduced electron injection from Ag into AgCl.[31] As shown in Fig. 4, moreover, the highly dispersive CB and VB provide favourable support to facilitate the transport of photoinduced charge carriers, which is an significant process for photocatalysis.

The synergistic effect between metallic Ag NPs and the n-type AgCl semiconductor introduces several significant improvements to the red Ag/AgCl photocatalytic system.[1] First, the featured LSPR brings several significant benefits: (i) drastically enhances the visible-light absorption, (ii) creates an intensive local electric field, (iii) powers the excitation of charge carries.[15, 52] Second, the Schottky junction resulted from the contact of Ag and AgCl, builds up an internal electric field in the space-charge region, which considerably enhances the separation of the photoinduced charge carries and suppresses their recombination.[1, 53] Third, the surface plasmon induces the polarization effect which enhances the adsorption and localized heating effect which boosts the reaction rate and benefits the mass transfer.[3, 54-56] To sum up, the optical absorption and utilization efficiency, local electric field, generation and separation of photoinduced charge carries, temperature dependence, interaction with molecules, *etc.* are greatly enhanced within the Ag/AgCl photocatalytic system.[57] In addition to the intrinsic properties, the higher photoactivity of the red AgCl photocatalysts can also be ascribed to its larger surface area (1.673 m^2/g for red AgCl and 1.382 m^2/g for normal AgCl, see ESI, Fig. S4†).

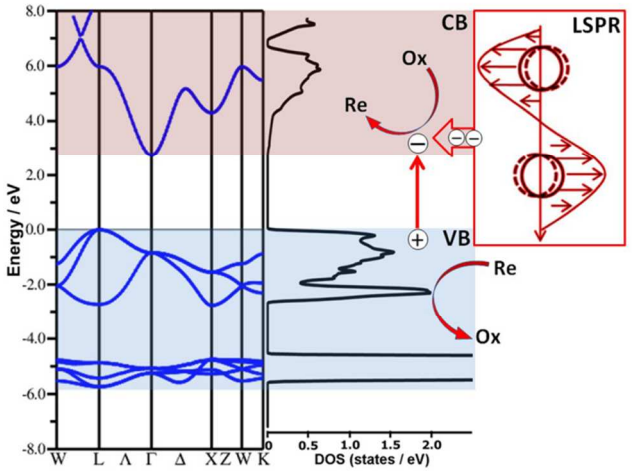

Fig. 4 A schematic illustration of the physical photocatalytic mechanism of the Ag/AgCl system. Band structures (left panel) and density of states (right panel) of the red Ag/AgCl photocatalyst.

As illustrated in Fig. 4, when the red Ag/AgCl photocatalysts are subjected to visible light irradiation, generation of electrons and holes is boosted by means of LSPR. The increased electron density disequilibrates the Fermi level and thus impels the energetic electron-transfer from Ag to the CB of AgCl.[10] During the photocatalytic process, nonpolar reactant molecules (CO_2) are polarized and polar molecules (MO and Cr^{VI}) are activated for better adsorption by the surface plasmon.[56] Then the adsorbed oxides are reduced directly with the electrons, while the oxidation are catalyzed directly by holes or by the reactive oxidative species ($O_2^{\cdot-}$, H_2O_2 and Cl^0) which are resulted from the electrons.[1, 10]

Conclusions

In summary, a novel kind of red Ag/AgCl photocatalysts with uniform coaxial tri-cubic morphology is prepared *via* a facile and versatile approach. The optical absorption of the as-prepared red photocatalysts is significantly enhanced, which is not only ascribed to the synergy of Ag and AgCl but also attributed to the Mie scattering effect due to the distinct morphology. Experimental results show that the red Ag/AgCl photocatalysts exhibit highly efficient photocatalytic oxidative and reductive ability in terms of degradation of MO and reduction of Cr^{VI} and CO_2. This work provides a novel perspective for understanding the physical photocatalytic mechanism of the red Ag/AgCl system and should stimulate the development of silver halide-based photocatalysts for the exploitation and utilization of solar energy.

Acknowledgements

The authors are most grateful to the NSFC, China (No.

21225524, 21175130, 21105096 and 21205112) and the Department of Science and Techniques of Jilin Province (No.20120308 and 201215091) for their financial support.

Notes and references

[a] *State Key Laboratory of Electroanalytical Chemistry, c/o Engineering Laboratory for Modern Analytical Techniques, Changchun Institute of Applied Chemistry, Chinese Academy of Sciences, Changchun 130022, Jilin, China. E-mail: lniu@ciac.ac.cn*

[b] *State Key Laboratory of Rare Earth Resource Utilization, Changchun Institute of Applied Chemistry, Chinese Academy of Sciences, Changchun 130022, Jilin, China.*

[c] *Graduate University of the Chinese Academy of Sciences, Beijing 100039, China.*

† Electronic Supplementary Information (ESI) available: Experimental details, additional Fig.s and discussions. See DOI: 10.1039/b000000x/

1. Z. Xuming, C. Yu Lim, L. Ru-Shi and T. Din Ping, *Rep Prog Phys*, 2013, **76**, 046401.
2. P. Wang, B. Huang, Y. Dai and M. H. Whangbo, *Phys Chem Chem Phys*, 2012, **14**, 9813-9825.
3. P. Christopher, H. Xin and S. Linic, *Nat. Chem.*, 2011, **3**, 467-472.
4. W. Hou and S. B. Cronin, *Adv Funct Mater*, 2013, **23**, 1612-1619.
5. N. Chandrasekharan and P. V. Kamat, *J Phys Chem B*, 2000, **104**, 10851-10857.
6. P. V. Kamat, *J Phys Chem B*, 2002, **106**, 7729-7744.
7. Y. Tian and T. Tatsuma, *Chem Commun*, 2004, **0**, 1810-1811.
8. K. Awazu, M. Fujimaki, C. Rockstuhl, J. Tominaga, H. Murakami, Y. Ohki, N. Yoshida and T. Watanabe, *J Am Chem Soc*, 2008, **130**, 1676-1680.
9. Z. Zhang and J. T. Yates, Jr., *Chem Rev*, 2012, **112**, 5520-5551.
10. B. Cai, X. Lv, S. Gan, M. Zhou, W. Ma, T. Wu, F. Li, D. Han and L. Niu, *Nanoscale*, 2013, **5**, 1910-1916.
11. P. Wang, B. Huang, X. Qin, X. Zhang, Y. Dai, J. Wei and M. H. Whangbo, *Angew Chem Int Ed*, 2008, **47**, 7931-7933.
12. Z. W. Seh, S. H. Liu, M. Low, S. Y. Zhang, Z. L. Liu, A. Mlayah and M. Y. Han, *Adv Mater*, 2012, **24**, 2310-2314.
13. Z. Wang, J. Liu and W. Chen, *Dalton Trans*, 2012, **41**, 4866-4870.
14. I. Thomann, B. A. Pinaud, Z. Chen, B. M. Clemens, T. F. Jaramillo and M. L. Brongersma, *Nano Lett*, 2011, **11**, 3440-3446.
15. T. Torimoto, H. Horibe, T. Kameyama, K.-i. Okazaki, S. Ikeda, M. Matsumura, A. Ishikawa and H. Ishihara, *J. Phys. Chem. Lett.*, 2011, **2**, 2057-2062.
16. C. Hu, T. W. Peng, X. X. Hu, Y. L. Nie, X. F. Zhou, J. H. Qu and H. He, *J Am Chem Soc*, 2010, **132**, 857-862.
17. D. H. Zhang, G. D. Li, J. X. Li and J. S. Chen, *Chem Commun*, 2008, 3414-3416.
18. H. Wang, T. T. You, W. W. Shi, J. H. Li and L. Guo, *J Phys Chem C*, 2012, **116**, 6490-6494.
19. K. Kimura, S. Naya, Y. Jin-nouchi and H. Tada, *J Phys Chem C*, 2012, **116**, 7111-7117.
20. Y. Ma, Q. Xu, X. Zong, D. G. Wang, G. P. Wu, X. Wang and C. Li, *Energ Environ Sci*, 2012, **5**, 6345-6351.
21. E. Formo, E. Lee, D. Campbell and Y. Xia, *Nano Lett*, 2008, **8**, 668-672.
22. J. Kim, D. Monllor-Satoca and W. Choi, *Energ Environ Sci*, 2012, **5**, 7647.
23. H. Tong, S. Ouyang, Y. Bi, N. Umezawa, M. Oshikiri and J. Ye, *Adv Mater*, 2012, **24**, 229-251.
24. N. Kakuta, N. Goto, H. Ohkita and T. Mizushima, *J Phys Chem B*, 1999, **103**, 5917-5919.
25. P. Wang, B. Huang, X. Zhang, X. Qin, Y. Dai, Z. Wang and Z. Lou, *ChemCatChem*, 2011, **3**, 360-364.
26. H. Wang, X. Lang, J. Gao, W. Liu, D. Wu, Y. Wu, L. Guo and J. Li, *Chem Eur J*, 2012, **18**, 4620-4626.
27. C. An, S. Peng and Y. Sun, *Adv Mater*, 2010, **22**, 2570-2574.
28. C. An, J. Wang, W. Jiang, M. Zhang, X. Ming, S. Wang and Q. Zhang, *Nanoscale*, 2012, **4**, 5646-5650.
29. S. Ghosh, A. Saraswathi, S. S. Indi, S. L. Hoti and H. N. Vasan, *Langmuir*, 2012, **28**, 8550-8561.
30. Y. Bi and J. Ye, *Chem Commun*, 2009, **0**, 6551-6553.
31. Y. Tang, Z. Jiang, G. Xing, A. Li, P. D. Kanhere, Y. Zhang, T. C. Sum, S. Li, X. Chen, Z. Dong and Z. Chen, *Adv Funct Mater*, 2013, **23**, 2932-2940.
32. H. Wang, J. Yang, X. Li, H. Zhang, J. Li and L. Guo, *Small*, 2012, **8**, 2802-2806.
33. L. Han, Z. Xu, P. Wang and S. Dong, *Chem Commun*, 2013, **49**, 4953-4955.
34. P. Wang, B. Huang, X. Zhang, X. Qin, H. Jin, Y. Dai, Z. Wang, J. Wei, J. Zhan, S. Wang, J. Wang and M. H. Whangbo, *Chem Eur J*, 2009, **15**, 1821-1824.
35. Y. Bi, S. Ouyang, J. Cao and J. Ye, *Phys Chem Chem Phys*, 2011, **13**, 10071-10075.
36. M. R. Elahifard, S. Rahimnejad, S. Haghighi and M. R. Gholami, *J Am Chem Soc*, 2007, **129**, 9552-9553.
37. P. Wang, B. B. Huang, X. Y. Qin, X. Y. Zhang, Y. Dai and M. H. Whangbo, *Inorg Chem*, 2009, **48**, 10697-10702.
38. B. Amrani, F. El Haj Hassan and M. Zoaeter, *Physica B: Condensed Matter*, 2007, **396**, 192-198.
39. B. Cai, J. Wang, D. Han, S. Gan, Q. Zhang, Z. Wu and L. Niu, *Nanoscale*, 2013, DOI:10.1039/C1033NR03365A.
40. S. Peng and Y. Sun, *J Mater Chem*, 2011, **21**, 11644-11650.
41. S. L. Murov, G. L. Hug and I. Carmichael, *Handbook of Photochemistry*, Dekker, New York, 1973.
42. M. Schiavello, V. Augugliaro, V. Loddo, M. J. López-Muñoz and L. Palmisano, *Res Chem Intermediat*, 1999, **25**, 213-227.
43. K. Schwarz and P. Blaha, *Comp Mater Sci*, 2003, **28**, 259-273.
44. A. A. P. W. WIEN2k, *Schwarz, Technical University of Wien, Austria*, 2001.
45. J. P. Perdew, K. Burke and Y. Wang, *Phys Rev B*, 1996, **54**, 16533-16539.
46. A. I. Liechtenstein, V. I. Anisimov and J. Zaanen, *Phys Rev B*, 1995, **52**, R5467-R5470.
47. Y. Bi, S. Ouyang, N. Umezawa, J. Cao and J. Ye, *J Am Chem Soc*, 2011, **133**, 6490-6492.
48. S. Glaus and G. Calzaferri, *Photochem. Photobiol. Sci.*, 2003, **2**, 398-401.
49. X. X. Xu, C. Randorn, P. Efstathiou and J. T. S. Irvine, *Nat Mater*, 2012, **11**, 595-598.
50. M. Gaberell, Y.-P. Chin, S. J. Hug and B. Sulzberger, *Environ Sci Technol*, 2003, **37**, 4403-4409.
51. C. An, J. Wang, C. Qin, W. Jiang, S. Wang, Y. Li and Q. Zhang, *J Mater Chem*, 2012, **22**, 13153-13158.
52. S. Mubeen, G. Hernandez-Sosa, D. Moses, J. Lee and M. Moskovits, *Nano Lett*, 2011, **11**, 5548-5552.
53. Z. Wang, J. Liu and W. Chen, *Dalton Trans*, 2012, **41**, 4866-4870.
54. J. R. Adleman, D. A. Boyd, D. G. Goodwin and D. Psaltis, *Nano Lett*, 2009, **9**, 4417-4423.
55. X. Chen, H.-Y. Zhu, J.-C. Zhao, Z.-F. Zheng and X.-P. Gao, *Angew Chem Int Ed*, 2008, **47**, 5353-5356.
56. X. Chen, H. Y. Zhu, J. C. Zhao, Z. F. Zheng and X. P. Gao, *Angew Chem Int Ed Engl*, 2008, **47**, 5353-5356.
57. Y. Nishijima, K. Ueno, Y. Yokota, K. Murakoshi and H. Misawa, *J Phys Chem Lett*, 2010, **1**, 2031-2036.

Graphical and textual abstract

A distinctive red Ag/AgCl photocatalyst with efficient photocatalytic oxidative and reductive activity

Bin Cai,[a,c] Jing Wang,[b,c] Shiyu Gan,[a,c] Dongxue Han,[a] Zhijian Wu,[b] and Li Niu*[a]

Keywords: photocatalysis; plasmonic; CO_2 photoreduction; hexavalent chromium; dye degradation

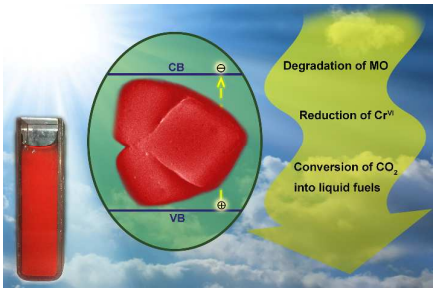

A large improvement of visible-light harvesting is obtained upon a distinctive kind of coloured Ag/AgCl photocatalyst.
